Fast-ion stabilization of tokamak plasma turbulence

A. Di Siena,[1] T. Görler,[1] H. Doerk,[1] E. Poli,[1] and R. Bilato[1]

[1] *Max Planck Institute for Plasma Physics, Boltzmannstr.2, 85748 Garching, Germany*

(Dated: July 3, 2018)

A significant reduction of the turbulence-induced anomalous heat transport has been observed in recent studies of magnetically confined plasmas in the presence of a significant fast-ion fractions. Therefore, the control of fast-ion populations with external heating might open the way to more optimistic scenarios for future fusion devices. However, little is known about the parameter range of relevance of these fast-ion effects which are often only highlighted in correlation with substantial electromagnetic fluctuations. Here, a significant fast ion induced stabilization is also found in both linear and nonlinear electrostatic gyrokinetic simulations which cannot be explained with the conventional assumptions based on pressure profile and dilution effects. Strong wave-fast particle resonant interactions are observed for realistic parameters where the fast particle trace approximation clearly failed and explained with the help of a reduced Vlasov model. In contrast to previous interpretations, fast particles can actively modify the Poisson field equation – even at low fast particle densities where dilution tends to be negligible and at relatively high temperatures, i.e. $T < 30T_e$. Further key parameters controlling the role of the fast ions are identified in the following and various ways of further optimizing their beneficial impact are explored. Finally, possible extensions into the electromagnetic regime are briefly discussed and the relevance of these findings for ITER standard scenarios is highlighted.

PACS numbers: 52.65.Tt

Increasing the energy confinement time is an absolutely crucial task for efficient magnetic confinement in nuclear fusion devices, such as tokamaks and stellarators. The main adversary is plasma turbulence which is driven by steep temperature and density gradients. Any mechanism limiting its development is therefore extremely valuable and should be taken into account in designing future devices. In this context, fast ions – in nowadays experiments created by the auxiliary plasma heating systems such as neutral beam injection (NBI) and ion cyclotron resonance heating (ICRH) – have attracted recent interest. While previous research has mainly focused on the possible excitation and impact of energetic particle driven modes, a few numerical and experimental studies [1–4] have hinted at fast particle effects on microturbulence. A prominent example is the ion temperature gradient (ITG) driven turbulence [5] which is held particularly responsible for the degradation of the ion energy confinement. The main electrostatic effect associated with the presence of fast ions is expected to be the dilution of the main ion species [1]. This effect depends only on the fast particle charge concentration. In low density regimes the fast particle dynamics is not expected to contribute in any way to the perturbed electrostatic potential and often in gyrokinetic simulations the trace approximation is used [6, 7]. This is justified by the fact that for low density the interaction of fast particles with the thermalized species is practically negligible. However, in certain situations fast particle effects on the microinstabilities could even be observed at low densities. For instance, a significant variation of the linear GYRO growth rates has been observed in presence of fast particles, suggesting an additional interaction mechanism which cannot be explained by dilution [3]. In several experiments [8, 9] significant improvement in the plasma confinement was observed and at first attributed to the combined effect of high rotational shear and low magnetic shear. Only afterwards, on the same set of discharges, numerical studies [10] have proven that turbulence suppression is linked to the inclusion of fast ions. Their role is often related to nonlinear, electromagnetic turbulence stabilization. In this Letter, a strong dynamic effect of fast particles on the plasma microinstability is shown to exist also in a linear, electrostatic setup. Fast particles can contribute to the development of turbulence modifying the main ion response to temperature and density gradients even at low density and high temperatures through a wave-particle resonance mechanism [11, 12]. This dynamic effect depends strongly on temperature and temperature gradient of the energetic-ion species and is observed to carry over to the fully electromagnetic case. Both, numerical results obtained with the gyrokinetic code GENE [13] and a reduced theoretical Vlasov model are presented in this Letter. Our explanation clarifies for the first time how fast ions mitigate microturbulence and suggests a possible way to control and optimize their beneficial impact. The importance of the aforementioned effect for an ITER standard scenario is addressed with linear and nonlinear GENE simulations.

The plasma parameters considered in the first part of this study, see Tab. I, are taken from a JET L-mode discharge with both NBI and ICRF heating [8, 9] and with substantial fast ion effects [10]. To facilitate the analysis, only a single fast particle species described by a Maxwellian distribution function with an equivalent temperature – e.g., either NBI fast deuterium or ICRH ^3He

– will be retained at a time while the bulk plasma is composed of deuterium and electrons. The simulations are furthermore performed in a fluxtube domain justified by the small Larmor-radius-to-minor-radius ratio evaluates to $\rho_i^* = 1/450$ for thermal ions and $\rho^*_{fast,D} = 1/150$; $\rho^*_{^3He} = 1/200$, respectively, for fast deuterium and helium. All simulations are performed in the electrostatic limit unless noted otherwise and with numerical Miller [14] equilibrium.

TABLE I. Parameters for the JET L-mode discharge 73224 [10, 15] ($\rho_{\rm tor} = 0.33$) and the ITER standard scenario ($\rho_{\rm tor} = 0.32$). Here, T denotes the temperature normalized to the electron one, $R/L_{T,n}$ the normalized logarithmic temperature and density gradients, $\hat{s}$ the magnetic shear and ν^* the electron-ion collision frequency normalized to the trapped electron bounce frequency.

JET							
R/m	$\hat{s}$	q	T_i	R/L_{T_i}	R/L_{T_e}	R/L_{n_e}	ν^*
3.1	0.5	1.7	1.0	9.3	6.8	1.3	0.038
n_{fD}	$n_{^3He}$	T_{fD}	$T_{^3He}$	$R/L_{T_{fD}}$	$R/L_{T_{^3He}}$	R/L_{nfD}	$R/L_{n_{^3He}}$
0.06	0.07	9.8	6.9	3.2	23.1	14.8	1.6

ITER						
R/m	$\hat{s}$	q	T_D	T_T	R/L_{T_D}	R/L_{T_T}
6.2	0.27	1.12	0.74	0.74	1.96	1.87
$n_{^3He}$	$R/L_{n_{^3He}}$	R/L_{n_T}	R/L_{n_D}	R/L_{n_e}	R/L_{T_e}	ν^*
0.03	0.6	0.6	0.6	0.6	1.26	0.0

The linear growth rate normalized to c_s/a with $c_s = (T_e/m_i)^{1/2}$ and minor radius a is shown in Fig. 1 as a function of (a) the fast ^3He and (b) the fast deuterium temperature. All linear GENE simulations presented here have been performed at a fixed wave number of $k_y\rho_s = 0.5$ where the maximum ITG linear growth rate is observed. A striking feature in Fig. 1 is the particularly strong dependence of the linear growth rate on the fast ^3He temperature. A pronounced reduction is found around $T_f \sim 12T_e$ with 50% growth rate amplitude compared to the case without fast particles and still 30% compared to a pure dilution case, obtained neglecting fast ions only in the first order quasineutrality equation. For the fast deuterium case a slowly monotonic growth-rate reduction is found, with $\sim 20\%$ at $T > 39T_e$. The fast particles add a positive contribution to the main ITG drive which rapidly decays to zero when the fast particle temperature is increased. Again, dilution is recovered at very high temperatures which could imply that highly energetic fusion alpha particles, i.e. $T \sim 80T_e$, may be described by dilution only [16]. The magnitude of the fast ion contribution to the overall ITG growth rate is found to scale linearly with the fast ion charge concentration. A reduced collisionless Vlasov model has been developed to explain and predict the main physical mechanisms involved in this significant fast particle stabilizing effect. By starting from the fast-particle

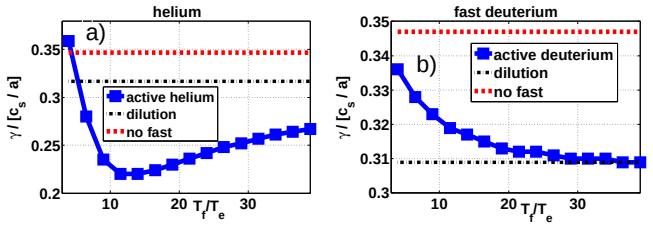

FIG. 1. Growth rates as function of T_f/T_e a) fast helium and b) fast deuterium.

electrostatic Vlasov equation without the trapping, the radial-curvature and the parallel-dynamic contributions, which are negligible [12], and by employing the plane wave ansatz for the perturbed quantities [17, 18] we arrive at

$$F_1 = \frac{k_y\phi_1\left[\frac{1}{2v_{\shortparallel}}\frac{\partial F_0}{\partial v_{\shortparallel}}\left(\frac{\mu B_0+2v_{\shortparallel}^2}{B_0}\right)\mathcal{K}_y - \frac{1}{C}\hat{\partial}_x F_0\right]}{\omega_r + i\omega_i + \frac{T_f}{q}\left(\frac{\mu B_0+2v_{\shortparallel}^2}{B_0}\right)k_y\mathcal{K}_y} \qquad (1)$$

which is written in normalized units and in field-aligned coordinates with the radial coordinate x, the binormal coordinate y, and the parallel coordinate z [19]. The velocity space is represented by the velocity parallel to the magnetic field $v_{\shortparallel}$ normalized to the species' thermal velocity $v_{th} = (2T/m)^{1/2}$ and the magnetic moment μ normalized to T/B_0 with reference magnetic field B_0 taken on axis. Furthermore, C is defined through the relation $\mathbf{B}_0 = C\nabla x \times \nabla y$ and $\mathcal{K}_y = -2((\mathbf{B}_0 \times \nabla B_0)\cdot\hat{y})/B_0^2$. To give an example, these quantities evaluate to $C = \mathbf{B}_0\cdot\mathbf{B}_0$ and $\mathcal{K}_y \sim -\cos(\theta) - \hat{s}\theta\sin(\theta)$ for a simple $\hat{s}-\alpha$ magnetic equilibrium. Here, positive values of the real frequency ω_r identify a mode propagating in the ion direction. The wave-fast-ion resonance corresponds to the condition that the denominator in (1) is zero. If a Maxwellian background distribution function is chosen, its derivatives evaluate to

$$\hat{\partial}_x F_{0,M} = \left[\frac{R}{L_n} + \frac{R}{L_T}\left(v_{\shortparallel}^2 + \mu B_0 - \frac{3}{2}\right)\right]F_{0,M} \qquad (2)$$

and $1/(2v_{\shortparallel})\partial F_0/\partial v_{\shortparallel} = -F_0$ in normalized units. According to Eq. (1), the main contributions to the fast-particle distribution F_1 stem from the background drive term (temperatures and density gradients) and from the y-curvature term. These results are in agreement with [11, 12] and are further validated below against full numerical simulations. A certain fraction of fast particles can resonate with the bulk-ion microinstability when the real part of the denominator of Eq. (1) is zero, i.e. when the magnetic-drift velocity matches the propagation velocity of the mode. In order for this condition to occur, $\mathcal{K}_y$ must be negative, which is the case on the outboard side of the tokamak. The velocity and poloidal dependency - identified by the angle θ - of the wave-fast particle

resonance can be studied with both the reduced Vlasov model and GENE simulations here retaining helium as a fast-particle species and neglecting collisions in order to facilitate comparisons. The latter choice is also justified by simulation based observations that collisions seem to have negligible impact on the resonant fast particle stabilizing mechanism studied in this Letter – possibly due the relatively high bulk ion temperature and low fast ion density. In Fig. 2 the real part of F_1/ϕ_1 is shown in the $v_{\shortparallel} - \theta$ plane for different values of the magnetic moment μ. For small values of the magnetic moment, a resonance can be identified for a broad range of $v_{\shortparallel} - \theta$ values with a maximum at $\theta = 0$ (Fig. 2a). Increasing μ, smaller values of $\mathcal{K}_y$ and $v_{\shortparallel}$ are required for the fast particle drift velocity to match the linear ITG mode propagation velocity. In the case of large μ, the resonance condition can be satisfied only at the edge of the bad-curvature region, i.e. $\theta \sim \mp 1.8$ (Fig. 2b). These results are well reproduced by the reduced Vlasov model.

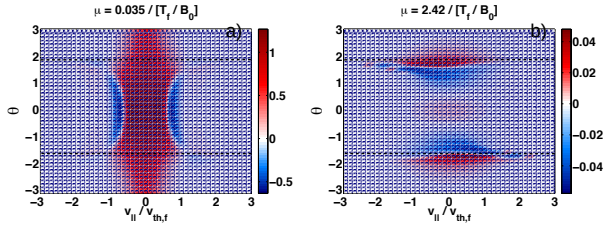

FIG. 2. Real part of F_1/ϕ_1 in the $v_{\shortparallel} - \theta$ space at $T_f = 12T_e$ for $\mu = 0.035$ (a) and 2.42 (b) from GENE. In the θ-region enclosed by the black dotted lines $\mathcal{K}_y < 0$ and positive elsewhere.

The contribution of the fast particles to the overall microinstability growth rate can be investigated in velocity space through the energy conservation property of the Vlasov-Poisson equations [20–22]

$$\gamma_f(v_{\shortparallel}, \mu) = -\frac{1}{E_{pot}} \int \pi B_0 \left(v_{\shortparallel}^2 + \mu B_0\right) \frac{\partial F_1}{\partial t} d^3x \qquad (3)$$

where E_{pot} denotes the potential energy. Employing the plane wave ansatz and considering the simplified F_1 distribution derived in Eq. (1), Eq. (3) shows that the phase space structure of γ_f is mainly determined by the background drive term and by the wave-particle resonance. This is also confirmed in actual GENE results as shown in Fig. 3. In the thermal limit ($T_f = T_e$), the velocity space structure of the helium growth rate contribution is predominantly determined by the drive term since the resonance condition is only met at large velocities where the drive term is small. This picture changes with increasing fast ion temperature. While the drive term, with stabilizing (negative) components at $v_{\shortparallel}^2 + \mu B_0 < 3/2$ and destabilizing (positive) components elsewhere, does not change in the given normalization, the resonance condition moves to smaller velocities when the fast-ion temperature is increased, as depicted in Fig. 3a. The resulting contribution of helium to the growth rate is hence more and more dominated by the stabilizing region of velocity space. The maximum stabilizing contribution is found when the helium temperature is such that the drift velocity of the mode matches the minimum in the drive term as expressed by Eqs. (2,3). This sweet spot is found around $T_f/T_e = 12$, see Fig. 3b. The findings in Fig. 1a can therefore be interpreted both qualitatively and quantitatively as results of the combined drive and wave-fast ion interaction on the helium contribution of the overall growth rate. From Eq. (3), to maximize the resonant stabilization on the ITG growth rate the relation $\eta_f^{-1} = \frac{R}{L_{n,f}} / \frac{R}{L_{T,f}} < 1.5$ must be fulfilled which is obtained in the limit of zero fast particle energy and corresponds to the minimum condition for a negative drive. As the ratio of the density and temperature gradients decreases, the fast particle resonant stabilization increases. This is confirmed by the absence of stabilizing effect due to fast deuterium apart from dilution, as in Fig. 1b. The ratio $\eta_f^{-1} \sim 5$ in this case and the fast deuterium drive term is positive for all energies. In summary, according to the model described, the stabilizing effect of the fast particles requires at the same time that (a) the minimum of the background drive term expressed by Eqs. (2,3) is negative (this being controlled by η_f^{-1}) and (b) the wave-fast-ion resonance and this negative region of the background drive overlap in phase space (the effect being maximum if the propagation velocity of the mode matches the minimum of the drive). The interplay of these two key ingredients is clearly shown in Fig. 4a. For the case of low fast-particle temperatures $T_f < 6T_e$, the wave-fast-ion resonance coincides with positive values of the drive in phase space. An increase in the temperature gradients, therefore, leads to a fast-ion induced *destabilization*. However, as soon as the fast ion resonance approaches the threshold condition identified above, i.e. $v_{\shortparallel}^2 + \mu B_0 < 3/2$, the fast helium contribution to the linear growth rate becomes negative and a strong ITG stabilization is observed. The latter increases with $R/L_{T,f}$ and is maximum for $T_f = 12T_e$. These results

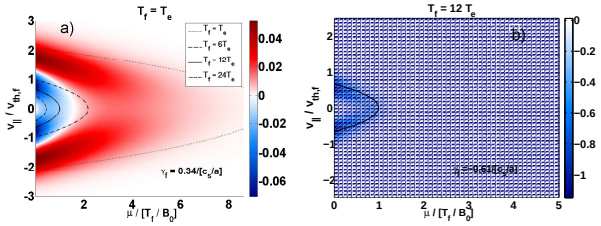

FIG. 3. Converged fast particle γ_f from GENE at low field side for (a) thermal and (b) $T_f = 12T_e$ helium. Black lines: resonance positions according to the reduced Vlasov model for different temperature ratios. Velocity space averaged growth rate contribution is included in the lower right of each plot.

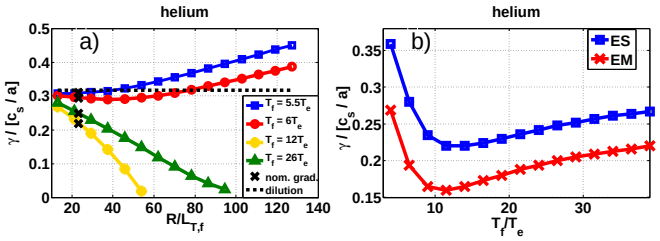

FIG. 4. Growth rates obtained (a) for different helium temperature and temperature gradients and (b) for electrostatic (blue line) and electromagnetic (red line) simulations.

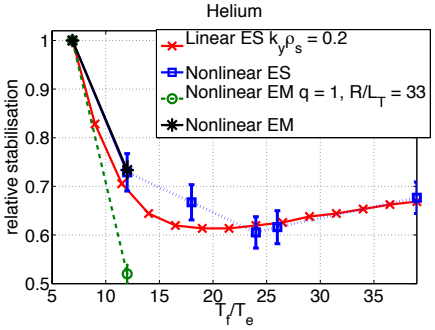

FIG. 5. Reduction of nonlinear ion heat fluxes and linear growth rates at $k_y\rho_s = 0.2$ for different helium temperatures and for $R/L_{T,f} = 33$ relative to their nominal values at $T_f/T_e = 6.9$: $\gamma^{\rm nom} = 0.163 c_s/a$, $q^{\rm nom}_{i,ES}/q_{gB} = 275.37$, $q^{\rm nom}_{i,EM}/q_{gB} = 100.39$, $q^{\rm nom}_{i,EM,q=1}/q_{gB} = 40.12$.

can be generalized to a fully electromagnetic framework. In Fig. 4b linear growth rates are shown for different fast-helium temperatures for a realistic ratio of the plasma to the magnetic pressure of $\beta_e = 0.33\%$. Qualitatively, the linear electromagnetic growth rates exhibit the same behaviour as the electrostatic ones while quantitatively they are found at lower values. The electrostatic stabilization seems to be not affected by finite beta effects. The electromagnetic fluctuations add an additional constant stabilization at each fast-particle temperature such that the combination of the two mechanisms may lead to a substantial microturbulence suppression. The same behaviour is observed for the fast deuterium setup.

The impact of the resonant fast-particle stabilization on turbulence is also studied with nonlinear simulations for the helium setup. The physics inputs are the same as indicated in Tab. I. The radial box size is $175\rho_s$ and the minimum $k_y\rho_s$ is set to 0.05. The grid numbers in direct space are $192 \times 96 \times 24$ in the radial, binormal and parallel directions while 20×32 grid points are used in the μ and the $v_{\shortparallel}$ velocity space dimensions. In Fig. 5 a comparison between the nonlinear main ion heat flux and the linear growth rate relative reduction is shown for different values of the fast-particle temperature. Linear growth rates and nonlinear main ion heat fluxes are normalized to the value at $T_f = 6.9T_e$ to study the additional resonant stabilization compared to the nominal temperature. For the linear simulations, $k_y\rho_s$ is set to 0.2 where the dominant heat transport spectrum component is found in the nonlinear simulations. Strong ITG suppression is observed in both linear and nonlinear simulations. An increase in the fast particle temperature leads to a strong reduction of the main ion heat transport which in the electrostatic simulations reaches values up to 40% at $T_f = 24T_e$ and seems to closely follow the trend of the linear growth rate at $k_y\rho_s = 0.2$. The wave-fast ion resonance interaction outlined above can therefore also be confirmed in nonlinear GENE turbulence simulations. This holds true for finite beta where the *relative* turbulence reduction at $T_f = 12T_e$ is almost identical with the electrostatic one. Although the dominant stabilizing mechanism is the nonlinear electromagnetic stabilization as it is clear from the absolute values mentioned in Fig. 5, the wave-fast ion resonance mechanism add another substantial turbulence reduction on top. Unfortunately, higher fast ion temperatures associated electromagnetic nonlinear resonant stabilization cannot be studied without crossing the KBM threshold [23]. However, a more pronounced ITG stabilization can, e.g., be obtained through a reduction of the safety factor $q = 1$ and an increase of the helium temperature gradient to $R/L_{T,f} = 33$. In this case a particularly strong ITG suppression of $\sim 50\%$ is observed. The latter can be further controlled by changing the fast-helium temperature and its gradient. In the remainder we discuss the impact of the wave-fast ion resonance stabilization on an ITER standard scenario with ^3He ICRH minority heating. In particular, we consider a time slice of the discharge just before the L-H transition [24], when the ion and electron temperatures are still low enough to have the ICRF waves mostly absorbed by the ^3He minority, and thus with a consistent fast-^3He population generated by ICRF heating (here we consider 3% of ^3He). For the temperatures foreseen at the flattop of the discharge (larger than 15 keV), ICRF waves are efficiently absorbed by tritium and electrons, and consequently the fast-^3He population is substantially reduced. Nevertheless, this initial phase of the discharge is essential for entering the flattop, and thus the present mechanism can play an important role in the initial phase of the ITER discharge. Realistic kinetic profiles for the thermal species - deuterium and tritium - and magnetic equilibrium have been extracted from JINTRAC simulations [24], see Tab. I. In Fig. 6 a corresponding linear and nonlinear analysis is performed for different ICRF injected power at the radial position $\rho_{tor} = 0.32$. The fast helium kinetic profiles are consistently computed with the ICRF full-wave TORIC code interfaced with the SSFPQL Fokker-Planck solver [25, 26]. As predicted by the wave-fast ion stabilizing mechanism described above, only a small fast ion contribution is ob-

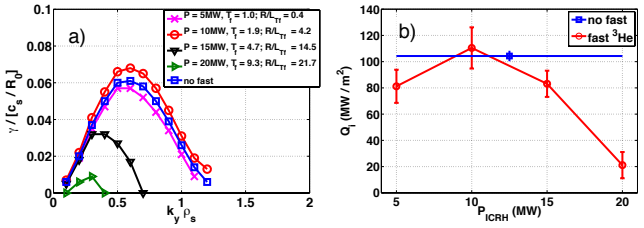

FIG. 6. Growth rates a) and nonlinear main ion heat flux b) as a function of $k_y\rho_s$ and injected ICRF power for an ITER standard scenario at $\rho_{tor} = 0.32$.

served for $P_{\mathrm{ICRH}} = 5\,\mathrm{MW}$, i.e. where the fast ion drive is practically negligible. An increase in the fast-ion temperature gradients, i.e. $P_{\mathrm{ICRH}} = 10\,\mathrm{MW}$, leads to a stronger fast ion contribution in the field equation, which however becomes destabilizing since the wave-fast-ion resonance is still in the positive region of the background drive. On the contrary, a significant reduction in both linear growth rates and nonlinear fluxes can be achieved for the case of $P = 20\,\mathrm{MW}$, i.e. where $T_f > 6T_e$ and the wave-fast ion resonance overlaps with the negative region of the background drive. For this case, fast ions add a substantial stabilizing contribution with a consequent overall ITG suppression, which is stronger at higher mode numbers. This result is consistent with Eq. (1). For smaller values of $k_y\rho_i$ the resonance condition can be satisfied only for higher fast ion temperatures.

In conclusion, fast ion dynamic effects on the main ion turbulence have been studied for realistic parameters and geometries via gyrokinetic GENE simulations and via a simplified analytic model to single out the most relevant physics mechanisms in the simulations. It is found that fast particles can strongly affect the main ion microinstabilities. Fast ions can interact with the main ion microinstability through a wave-particle resonance mechanism when the fast ion magnetic-drift frequency is close enough to the linear frequency of the wave. This mechanism can lead to a significant stabilization when the phase-space resonance position coincides with the beneficial (negative) region of the fast particle drive term. The main physical parameters controlling the impact of the fast ions are identified. Precisely, when the fast-ion temperature maximizes the stabilizing effect of the resonance and the temperature gradient exceeds the density gradient, strong ITG mode suppression can be expected. The latter condition is well matched by fast-ion tails created by ICRF heating. Nonlinear simulations demonstrate that turbulence suppression of $\sim 50\%$ is achievable by optimizing the wave-particle resonance. These mainly electrostatic findings are also confirmed in linear and nonlinear electromagnetic GENE simulations, and are in line with experimental evidences [8–10]. In this Letter, we propose and substantiate a physical explanation for the observed impact of the fast-ion population on the turbulence-induced transport and furthermore suggest criteria to improve the energy confinement by tailoring the fast-ion population with auxiliary heating. As exemplified by simulations with parameters typical to the ITER standard scenario, this may not only be relevant to present-day experiments but could also imply way more optimistic predictions for reactor-scale devices.

The simulations presented in this work were performed at the HYDRA HPC system at the Max Planck Computing and Data Facility (MPCDF), Germany. Furthermore, we acknowledge the CINECA award under the ISCRA initiative, for the availability of high performance computing resources and support. The authors would like to thank A. Zocco, J. Citrin, P. Lauber, F. Jenko, C. Angioni and M. Romanelli for all the stimulating discussions, useful suggestions and comments.

[1] G. Tardini, J. Hobirk, V. G. Igochine, C. F. Maggi, P. Martin, D. McCune, A. G. Peeters, A. C. C. Sips, A. Stäbler, J. Stober, and ASDEX Upgrade Team, Nucl. Fusion **47**, 280 (2007).
[2] M. Romanelli, A. Zocco, F. Crisanti, and JET Contributors, Plasma Phys. Controlled Fusion **52**, 045007 (2010).
[3] C. Holland, C. C. Petty, L. Schmitz, K. H. Burrell, G. R. McKee, T. L. Rhodes, and J. Candy, Nucl. Fusion **52**, 114007 (2012).
[4] J. Citrin, J. Garcia, T. Görler, F. Jenko, P. Mantica, D. Told, C. Bourdelle, D. R. Hatch, G. M. D. Hogeweij, T. Johnson, M. J. Pueschel, and M. Schneider, Plasma Phys. Controlled Fusion **57**, 014032 (2015).
[5] F. Romanelli, Physics of Fluids B **1**, 1018 (1989).
[6] C. Estrada-Mila, J. Candy, and R. E. Waltz, Phys. Plasmas **13**, 112303 (2006).
[7] T. Hauff and F. Jenko, Phys. Plasmas **15**, 112307 (2008).
[8] P. Mantica, D. Strintzi, T. Tala, C. Giroud, T. Johnson, H. Leggate, E. Lerche, T. Loarer, A. G. Peeters, A. Salmi, S. Sharapov, D. Van Eester, P. C. de Vries, L. Zabeo, and K.-D. Zastrow, Phys. Rev. Lett. **102**, 175002 (2009).
[9] P. Mantica, C. Angioni, C. Challis, G. Colyer, L. Frassinetti, N. Hawkes, T. Johnson, M. Tsalas, P. C. de Vries, J. Weiland, B. Baiocchi, M. N. A. Beurskens, A. C. A. Figueiredo, C. Giroud, J. Hobirk, E. Joffrin, E. Lerche, V. Naulin, A. G. Peeters, A. Salmi, C. Sozzi, D. Strintzi, G. Staebler, T. Tala, D. Van Eester, and T. Versloot, Phys. Rev. Lett. **107**, 135004 (2011).
[10] J. Citrin, F. Jenko, P. Mantica, D. Told, C. Bourdelle, J. Garcia, J. W. Haverkort, G. M. D. Hogeweij, T. Johnson, and M. J. Pueschel, Phys. Rev. Lett. **111**, 155001 (2013).
[11] C. Angioni and A. G. Peeters, Phys. Plasmas **15**, 052307 (2008).
[12] T. Dannert, S. Günter, T. Hauff, F. Jenko, X. Lapillonne, and P. Lauber, Phys. Plasmas **15**, 062508 (2008).
[13] F. Jenko, W. Dorland, M. Kotschenreuther, and B. N. Rogers, Phys. Plasmas **7**, 1904 (2000).
[14] R. Miller, M. Chu, J. Greene, Y. Lin-Liu, and R. Waltz, Phys. Plasmas **5**, 979 (1998).
[15] R. Bravenec, J. Citrin, J. Candy, P. Mantica, T. Görler,

and JET Contributors, Plasma Phys. Controlled Fusion **58** (2016), 10.1088/0741-3335/58/12/125018.
[16] G. J. Wilkie, I. G. Abel, E. G. Highcock, and W. Dorland, J. Plasma Phys. **81** (2015), 10.1017/S002237781400124X.
[17] J. W. Connor, R. J. Hastie, and J. B. Taylor, Phys. Rev. Lett. **40**, 396 (1978).
[18] M. Kotschenreuther, G. Rewoldt, and W. M. Tang, Comput. Phys. Commun. **88**, 128 (1995).
[19] T. Görler, X. Lapillonne, S. Brunner, T. Dannert, F. Jenko, F. Merz, and D. Told, Journal of Computational Physics **230**, 7053 (2011).
[20] R. Hatzky, T. M. Tran, A. Könies, R. Kleiber, and S. J. Allfrey, Phys. Plasmas **9**, 898 (2002).
[21] A. Bañón Navarro, P. Morel, M. Albrecht-Marc, D. Carati, F. Merz, T. Görler, and F. Jenko, Phys. Plasmas **18**, 092303 (2011).
[22] P. Manas, Y. Camenen, S. Benkadda, W. A. Hornsby, and A. G. Peeters, Phys. Plasmas **22**, 062302 (2015).
[23] M. J. Pueschel and Jenko, Phys. Plasmas **17**, 102310 (2010).
[24] V. Parail, R. Albanese, R. Ambrosino, J.-F. Artaud, K. Besseghir, M. Cavinato, G. Corrigan, J. Garcia, L. Garzotti, Y. Gribov, F. Imbeaux, F. Koechl, C. Labate, J. Lister, X. Litaudon, A. Loarte, P. Maget, M. Mattei, D. McDonald, E. Nardon, G. Saibene, R. Sartori, and J. Urban, Nucl. Fusion **53**, 113002 (2013).
[25] M. Brambilla and R. Bilato, Nucl. Fusion **49**, 085004 (2009).
[26] R. Bilato, M. Brambilla, O. Maj, L. Horton, C. Maggi, and J. Stober, Nucl. Fusion **51**, 103034 (2011).